

Influence of Nitrogen Flow Rates on the Structure, Hardness, and Electrical Resistivity of HfN Coatings by DC Sputtering

Leandro García-González, Luis Zamora-Peredo, Nelly Flores-Ramírez, María Guadalupe Garnica-Romo, and Julián Hernández-Torres

(Submitted June 4, 2014; in revised form December 22, 2014; published online February 7, 2015)

HfN hard coatings on Corning glass substrates were obtained using DC sputtering. A power of 200 W was used keeping the flow rate of argon at 10 sccm and varying the nitrogen flow rates at 2.5, 3.5, 5.0, and 7.5 sccm to analyze differences in the hardness and electrical resistivity values, explaining variations in relation to structural changes. To achieve this, the Vickers microhardness test, x-ray diffraction, Raman, atomic force microscopy, and high resistivity measurements were used. At 2.5 sccm, the hardness value was shown to reach a maximum value of 20 GPa, and a minimum electrical resistivity of $6.5 \times 10^8 \mu\Omega\text{cm}$. Furthermore, as the flow is increased, the hardness values gradually decrease (until a value of 8 GPa is reached), the fracture toughness increase (until a value of $0.3 \text{ MPa}\sqrt{\text{m}}$ is reached), and the electrical resistivity reaches its maximum at $1.52 \times 10^{12} \mu\Omega\text{cm}$. These variations are attributed to the evolution that the HfN phase progressively undergoes from a crystal orientation at (111) to an amorphous phase. In addition, the presence of tensile stresses, which tend to favor electrical resistivity, was identified. The average RMS roughness increased from 3.76 to 10.69 nm as the nitrogen flow was increased. Finally, the Raman spectroscopy confirmed the presence of the HfN phase.

Keywords electrical resistivity, HfN, sputtering, Vickers hardness, XRD

1. Introduction

Transition metals nitrides have been used as highly corrosion resistant materials, diffusion barriers in integrated circuits, and as protective coatings for industrial-type tools (Ref 1-3). There exist different ways to fabricate them, the most commonly used techniques being physical vapor deposition (PVD) (Ref 4, 5) and chemical vapor deposition (CVD) (Ref 6, 7). The sputtering technique has been one of the most commonly used methods to obtain nitrides, because of its versatility (Ref 8, 9). One of the most well-known and studied in recent years metal nitrides is titanium nitride (TiN) (Ref 10, 11), which has been widely used as a hard coating due to its high wear resistance, high hardness values, low friction coefficient, and very attractive appearance to the naked eye (Ref 12, 13). Both the mechanical and electrical properties of titanium nitride and in general of most nitrides strongly depend

on the growth conditions used in the sputtering process. The origin of this dependence may be associated with the defects contained within the coating, originated during growth. One of the main influences of the defects in the coating is caused by the oxygen concentration which significantly affects the titanium nitride's properties (Ref 14).

It has now been found that hafnium nitride (HfN) exhibits very similar properties to those of TiN (Ref 15). However, HfN also exhibits other properties such as a high melting point, chemical inertness, good oxidation resistance in external environments, high refractoriness, and especially an excellent electrochemical immunity and biocompatibility with the human body so as to be used in biomedical implants (Ref 16). To date, only few studies have been reported on the HfN binary system, of which approximately 20% have been obtained by DC sputtering (Ref 17, 18) and the rest by RF sputtering and other techniques such as vacuum plasma spraying or CVD (Ref 19-22). However, none of these studies using DC sputtering is aimed at studying the relationship between Vickers microhardness, fracture toughness, and electrical resistivity, and explaining its evolution through changes in its structure. Consequently, this paper focuses on proposing growing conditions favoring electrical resistivity, Vickers microhardness, and fracture toughness at different nitrogen flows and explaining these variations in terms of changes in its structure, phases, and stress involved.

Leandro García-González, Luis Zamora-Peredo, and Julián Hernández-Torres, Centro de Investigación en Micro y Nanotecnología, Universidad Veracruzana, Calzada Adolfo Ruiz Cortines, 455, Fracc. Costa Verde, Boca del Río, Veracruz, Mexico; **Nelly Flores-Ramírez**, Facultad de Ingeniería en Tecnología de la Madera de la Universidad Michoacana de San Nicolás de Hidalgo, Morelia, Michoacán, Mexico; and **Guadalupe Garnica-Romo**, Facultad de Ingeniería Civil, Universidad Michoacana de San Nicolás de Hidalgo, Morelia, Michoacán, Mexico. Contact e-mails: lgarcialegz@yahoo.com.mx.

2. Experimental

HfN hard coatings were produced on Corning glass substrates by DC sputtering using a V3 Model Intercovamex sputtering equipment and a 99.9% purity hafnium target. The

Corning glass substrates were cleaned in an ultrasonic bath using distilled water and soap, acetone, and ethanol. Once the pressure was pumped to 1.6×10^{-6} Torr, we proceeded to initiate growth of the coatings, using a flow rate of argon of 10 sccm and a power of 200 W until a thickness of 0.33 μm at room temperature was reached, varying the nitrogen gas flow rates in 2.5, 3.5, 5.0, and 7.5 sccm, identified as HfN-2.5, HfN-3.5, HfN-5.0, and HfN-7.5, severally. The values of the working pressure were of 1.6×10^{-2} , 2.2×10^{-2} , 2.7×10^{-2} , and 4.5×10^{-2} Torr for HfN-2.5, HfN-3.5, HfN-5.0, and HfN-7.5 coatings, respectively.

In order to analyze the microhardness of the hafnium nitride coatings on Corning glass substrates a Mitutoyo Vickers Microhardness tester was used applying loads of 0.001, 0.002, 0.003, 0.004, 0.005, 0.01, 0.025, 0.05, 0.1, 0.2, 0.3, and 0.5 Kgf, and repeating the measurement at least five times in different regions of the coating. The structure of the coatings was analyzed using a x-ray diffractometer (XRD) model D8 Advance from Bruker, using the copper $K_{\alpha 1}$ x-ray line, using a grazing incidence angle arrangement combined with a parallel beam geometry, as well as a scintillation detector, also applying a 2θ sweep range from 25° to 80° and 1° steps, with a step size of 0.02° and a speed of 2 s per step. The current and voltage used were 40 mA and 40 kV, respectively. The vibrational modes of the HfN coatings were analyzed using a Thermo Scientific DXR Raman microspectrometer with a $10\times$ objective, a collection time of 2 s, a sampling number of 10 s, and a solid-state laser beam with an excitation line of 532 nm at a power of 10 mW. The measurements of the surface morphology of the films were performed using a Digital Instruments atomic force microscope (AFM)—Nanoscope IV Dimension 3100. Finally, the electrical resistivity of the coatings was analyzed with a Keithley high resistance measurement equipment (Model 65) using different voltage values (5, 10 and 20 V) applying Ohm's law.

3. Results and Discussion

During the sputtering process, once the nitrogen gas has been incorporated into the growth chamber, the gas reacts with the hafnium target atoms, thereby forming hafnium nitride. For most transition metals, when the nitrogen flow rate is varied, a nonlinear behavior is observed in the material with respect to the reagent gas supply, showing a hysteresis effect (Ref 23). Usually when the nitrogen flow rate is small, the target material hardly reacts during the deposition process carried out on the Corning glass substrate, tending to reveal a behavior similar to that found in a metal eroding process. In contrast, when dealing with hafnium, the deposition rate to form HfN is high enough (Ref 15). In order to ensure the formation of HfN, the lowest value of nitrogen flow rate used was 2.5 sccm. When using smaller deposition rates, the hafnium would not reach a nitride phase and an unwanted Hf metal phase was observed in the diffractograms. As the nitrogen flow rate is increased, the erosion of the hafnium target decreases, consequently resulting in a longer time required to deposit the hafnium nitride of the same thickness. This is due to the performance of reactive sputtering, which is impeded by the effect of target "poisoning," which means that a compound coating is not only formed on the substrate as desired, but also on the sputter target, which results in a significantly reduced sputter yield and, thereby,

reduced deposition rate. When we eroded the hafnium target without the presence of nitrogen, the deposition rate was 2.8 $\text{K}\text{\AA}/\text{s}$. As we introduced the nitrogen reagent gas, we observed that the deposition rate decreased at 1.1, 0.6, 0.3, and 0.1 $\text{K}\text{\AA}/\text{s}$ at nitrogen flow rates of 2.5, 3.5, 5.0, and 7.5 sccm, respectively. For nitrogen flow rates higher than 10 sccm, the deposition process is hampered enormously, thus making it impossible to operate the sputtering process in an extremely reactive environment so as to reach a minimal deposition rate, in which the latter is practically null. This is primarily due to poisoning of the hafnium target, however, a further consequence of poisoning is a hysteresis of the reactive gas partial pressure at increasing/decreasing reactive gas flow, and, associated to this, an unstable operation regime between high and low target uptake at constant partial flow of the reactive gas. Furthermore, a decrease in the discharge voltage is also observed. Nonetheless, one of the advantages brought forth upon using these growth parameters in which the nitrogen reagent gas intervened, is that no electrical arcing occurred, which could have damaged both the hafnium target as well as the coating.

In Fig. 1, the peaks of x-ray diffraction for the set of four series of coatings produced by reactive DC sputtering on Corning glass substrates are displayed. When the nitrogen flow is introduced into the growth chamber, the appearance of the crystalline phase of hafnium nitride with a face-centered cubic structure (ICCD: 00-033-0592) can be identified in almost all coatings. At a nitrogen flow rate of 2.5 sccm, five diffraction peaks localized in $2\theta = 34.304^\circ$, 39.819° , 57.551° , 68.762° , and 72.282° can be very distinctly identified, which is related like a strong signal of stoichiometric HfN (Ref 17). When the nitrogen flow rate is increased, the intensity of the diffraction peaks corresponding to the FCC—HfN phase begin to decrease gradually until they are totally attenuated (HfN-7.5 coating with an amorphous phase). For the HfN-3.5 and HfN-5.0 coatings, the diffraction peak located at $2\theta = 72.282^\circ$ disappeared completely, but the crystal orientation remained constant along the (111) plane, which indicates that the coatings are close to stoichiometric HfN. The Warren-Averbach method (Ref 24) was used to calculate the grain size of the HfN-2.5, HfN-3.5, and HfN-5.0 coatings, using the diffraction profiles that reveal a polycrystalline behavior and a variation in the enlargement of

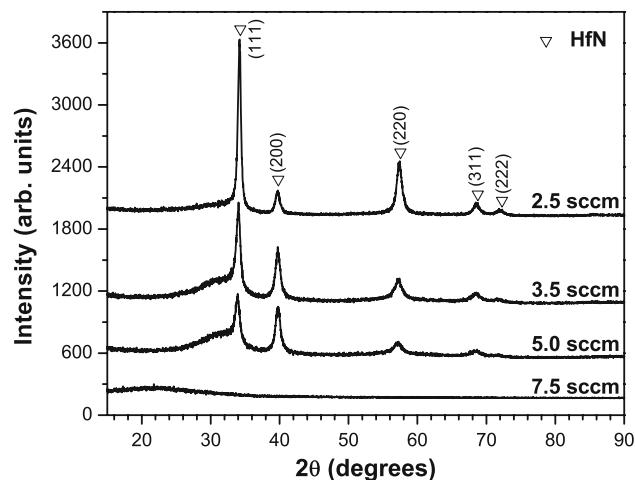


Fig. 1 X-ray diffraction pattern evolution with nitrogen flow rate of HfN coatings

the diffraction peaks. Our calculations show that there is little variation in the grain size values found for each coating, as they exposed values of 7.9, 8.3, and 9.1 nm for the HfN-5.0, HfN-3.5, and HfN-2.5 coatings, respectively.

Similarly, Fig. 1 shows that by increasing the nitrogen content, the lowest 2θ part of the (111) peak exhibits some shoulder probably due to the presence of an amorphous phase of hafnium oxide, and gradually becomes more evident, as the nitrogen flow rate is increased. The presence of oxygen is attributed to the contamination that remains on the walls of the sputtering deposition chamber due to the vacuum conditions used in the fabrication of the coatings (Ref 25).

In Fig. 2, the XRD data of the crystalline coatings are shown for the range of 32.5° to 36° in 2θ , in which we can observe that the peaks of most intense diffraction for the three coatings of HfN show a shift toward the left of the HfN base reference line, which was identified by x-ray diffraction. This result qualitatively could indicate that the three coatings show tensile stress, due to an increase in the amount of oxygen into the coatings. However, the effect of the stoichiometry of HfN is not discarded in the shift of the diffraction peaks. The shift is smaller for the nitrogen flow rate of 2.5 sccm and higher for the nitrogen flow rate of 5.0 sccm.

In Fig. 3, the Raman Spectra of the HfN-7.5 coating is depicted, and we can see approximately four wide bands centered at 163, 525, 670, and 1035 cm^{-1} . The first band corresponds to a first-order acoustic band ($115\text{--}180\text{ cm}^{-1}$) due to longitudinal acoustic phonons (LA) (Ref 17, 26). The second band is a first-order optical band ($480\text{--}560\text{ cm}^{-1}$) due to the first-order optical line (O) (Ref 17, 25). The third and fourth bands correspond to higher frequency bands located in lines at 670 and 1035 cm^{-1} , attributed to the sum of the acoustic and optical first-order modes (O + A) and to the second-order optical mode (2O), respectively (Ref 17, 26). For NaCl-structure compounds with no defects, the first-order Raman effect is forbidden by symmetry (Ref 26) and only second-order scattering is observed. From Raman Spectra, we can deduce that HfN coatings fabricated by DC sputtering have a NaCl-type structure. The presence of the first-order dispersion (LA and O) indicates the presence of point defect in the coatings (Ref 26). A similar behavior in the Raman signal is observed for all the coatings. However, by decreasing the nitrogen flow rate, the intensity of the Raman signals also decreases, which is

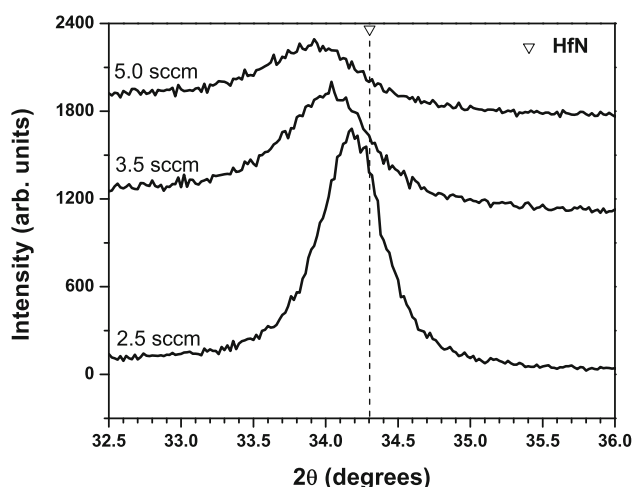


Fig. 2 X-ray diffraction of HfN coatings in the $32.5\text{--}36.0^\circ$ 2θ range

related to a decrease in the presence of the HfO phase (low number of point defects).

For the Vickers microhardness analysis of each coating, we used the Korsunsky's work-of-indentation model (Ref 27), which enables us to consider all the experimental data obtained in the experimental measurements made by the Vickers microindenter. This model is applicable to systems that behave plastically as well as to systems that tend to fracture which always depend upon the thickness of the coating. According to the model, the total work-of-indentation during the hardness testing comprises two components; one of the components is congruent with the work of plastic deformation in the substrate, and the other is congruent with the fracture energy of and/or deformation of the coating. Figure 4 shows the adjustment made to the 12 load values applied to the coating made with a nitrogen flow rate of 2.5 sccm, this coating being the one which scored the highest hardness value of 20 GPa. Upon adjusting, the evolution that the hardness undergoes in relation to the gradual change of the relative indentation depth due to different loads can be seen. The behavior displayed in Fig. 4, "knee" type, was predicted by the Korsunsky model, where for small load values, the curve tends

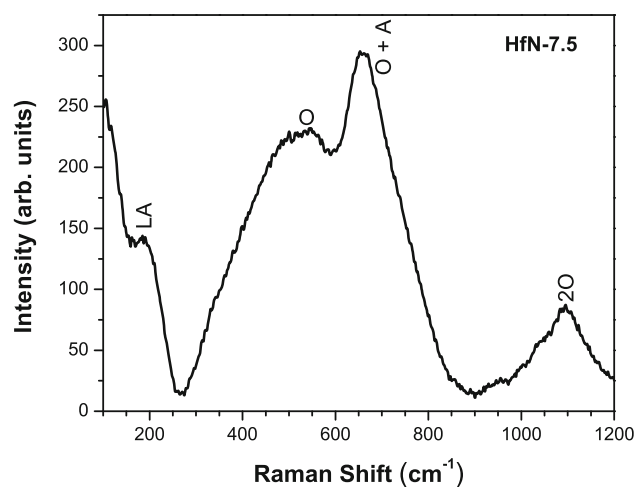


Fig. 3 Raman spectra of the HfN coating deposited at a nitrogen gas flow rate of 7.5 sccm

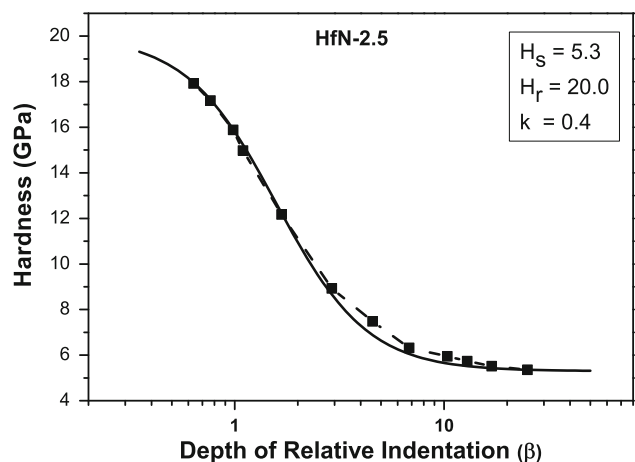


Fig. 4 Adjustment made to the coating HfN-2.5 using the model proposed by Korsunsky

to approach the value of the hardness of the coating, which dominates the plasticity of the coating; whereas for large load values, there is greater penetration and the curve approaches the value of the hardness of the substrate used, where the coating reaches fracture. In Fig. 5(a) and (b), we can observe the images of the indentations made to HfN coatings at two different loads. There are two remarkable effects to be noted in these images. First, critical loads values at which begin the formation of lateral cracks. Second, the formation of radial cracks at different load values. The radial cracks in HfN coatings were introduced by indenting them with a sharp Vickers indenter, and the relationship between the fracture toughness and the length of radial cracks was established. The load values, at which these cracks appear, can be seen in Table 1. For the 0.1 Kgf load and lower loads, no type of radial crack is evident and only the plastic effect can be seen, while for load values of 0.2, 0.3, and 0.5 Kgf (and higher values) the crack (radial or lateral) in the coating is initiated and visualized, progressively defining itself, as the load value is increased, as it is described in the Korsunsky model. The fracture toughness of HfN hard coatings was estimated using the radial cracking indentation method (ICL) by measuring the length of radial crack (Ref 28):

$$K_{IC} = Y \left(\frac{E_c}{H_c} \right)^{1/2} \frac{P}{C^{3/2}},$$

where C is the length of surface radial cracks, P the applied load, E_c ($= 380$ GPa) Young's modulus of HfN (Ref 29), H_c is the Vickers hardness measured in the coating, and Y is an empirical constant which depends on the geometry of the indenter used and the value is 0.016 for Vickers indenter (Ref 30). The results are shown in Table 1, corroborating that the coatings with higher fracture toughness are HfN-5.0 and HfN-7.5, because the coatings with lower hardness value presented higher fracture toughness, which means less brittleness.

Figure 6 shows the behavior of the Vickers microhardness and electrical resistivity of the coatings produced by the sputtering technique at different flows of nitrogen. As the nitrogen flow rate is increased, we can observe that the hardness values decrease, but the electrical resistivity values will gradually increase. The hardness will decrease from the maximum value of 20 GPa for the HfN-2.5 coating, until reaching the minimum value of 8 GPa, exhibited by the HfN-7.5 coating; while the electrical resistivity values start from a minimum value of $6.5 \times 10^8 \mu\Omega\text{cm}$ for HfN-2.5 and reach a maximum value of $1.52 \times 10^{12} \mu\Omega\text{cm}$ for HfN-7.5. The changes in hardness shown in Fig. 6 are attributed to microstructural changes and, favoring high hardness values to the higher crystallinity of the coating (stoichiometric HfN coating) and the unique formation of HfN phase, besides showing lower tensile stress. The maximum hardness value reached is similar to the values obtained by other researchers (Ref 18, 21). However, the difference is that they fabricated coatings by CVD and, as for us, we fabricated them by PVD. On the other hand, the microstructural and stoichiometric changes mentioned above also tended to affect the electrical resistivity, but in a way contrary to the behavior displayed in the hardness. The high values reached are mainly attributed to the amorphous phases with the highest tensile stresses, in addition to the dispersion of the point defects such as hafnium and nitrogen vacancies, and antisite defects. The two highest resistivity

values (1.86×10^{10} and $1.52 \times 10^{12} \mu\Omega\text{cm}$) are well above those reported by other researchers (Ref 17, 19, 31), who report values of $1 \times 10^8 \mu\Omega\text{cm}$ (using a nitrogen flow rate of 0.5) (Ref 17), $1.6 \times 10^8 \mu\Omega\text{cm}$ (using a 2% nitrogen flow rate without bias potential) (Ref 19), and $200 \mu\Omega\text{cm}$ (using a HfN target and varying the RF sputtering power supply) (Ref 31).

The hardness values are affected by the appearance of the amorphous phase of hafnium oxide, which becomes more evident as the nitrogen flow rate is increased along with a growing density of dislocations that are responsible for the relaxation of the coating and an increase in the root mean square of the roughness values from 3.76 to 10.69 nm. Figure 7 shows the image of the surface morphology of the HfN-2.5 coatings in an area of $5.0 \times 5.0 \mu\text{m}^2$ for a scanning speed of 1.0 Hz. As it may be seen, the coating consists of globular-shaped particles, where in the other coatings show a similar behavior.

When there is a greater presence of the reagent gas in the growth chamber, there is a higher internal pressure, which causes the coatings obtained to be more porous and therefore when they come in contact with the residual oxygen in the chamber, they rust faster. The hardest coating was grown at lower pressures, in such a way that it managed to be denser and less prone to oxidation, thereby obtaining a single well-defined crystalline phase of FCC—HfN, in contrast to other studies (Ref 17, 19, 32), where the phases of Hf_3N_2 , HfO_2 , Hf, and $\text{HfN}_{1.3}$, were found which affect not only the hardness values, but also the electrical resistivity.

4. Conclusions

It was possible to obtain coatings of HfN on glass substrates with a thickness of 333 nm through DC sputtering in a reactive atmosphere. As the nitrogen flow rate is increased, the erosion of the hafnium target decreases, due to the performance of reactive sputtering, which is impeded by the effect of target "poisoning." Using x-ray diffraction we could identify the presence of the HfN crystalline phase at nitrogen flow rates of 2.5, 3.5, and 5.0 sccm, being able to observe that the diffraction peaks have a crystal orientation at (111) and also display tensile stress. Raman measurements confirm the presence of bands related to the non-stoichiometric HfN phase, being the strongest for coatings with greater amounts of nitrogen. The value of maximum hardness achieved was 20 GPa, for a nitrogen flow rate of 2.5 sccm and as this flow rate is increased, the hardness values of the coating tend to decrease to a minimum value of 8 GPa, while electrical resistivity values start from a minimum value of $6.5 \times 10^8 \mu\Omega\text{cm}$ for HfN-2.5 and reach a maximum value of $1.52 \times 10^{12} \mu\Omega\text{cm}$ for HfN-7.5. The images of the indentation marks and the calculations of fracture toughness show that the coatings with higher fracture toughness are HfN-5.0 and HfN-7.5 coinciding with lower hardness values. This behavior is due to changes in the microstructure of the coatings, due to that the coating of higher hardness has a well-defined crystal structure, the lowest tensile stresses and the smaller contribution of an amorphous hafnium oxide phase. As the nitrogen flow rate increases progressively, the intensity of the diffraction peaks decreases and some even disappear ending up into a fully amorphous phase structure, favoring the high values of both electrical resistivity and fracture toughness.

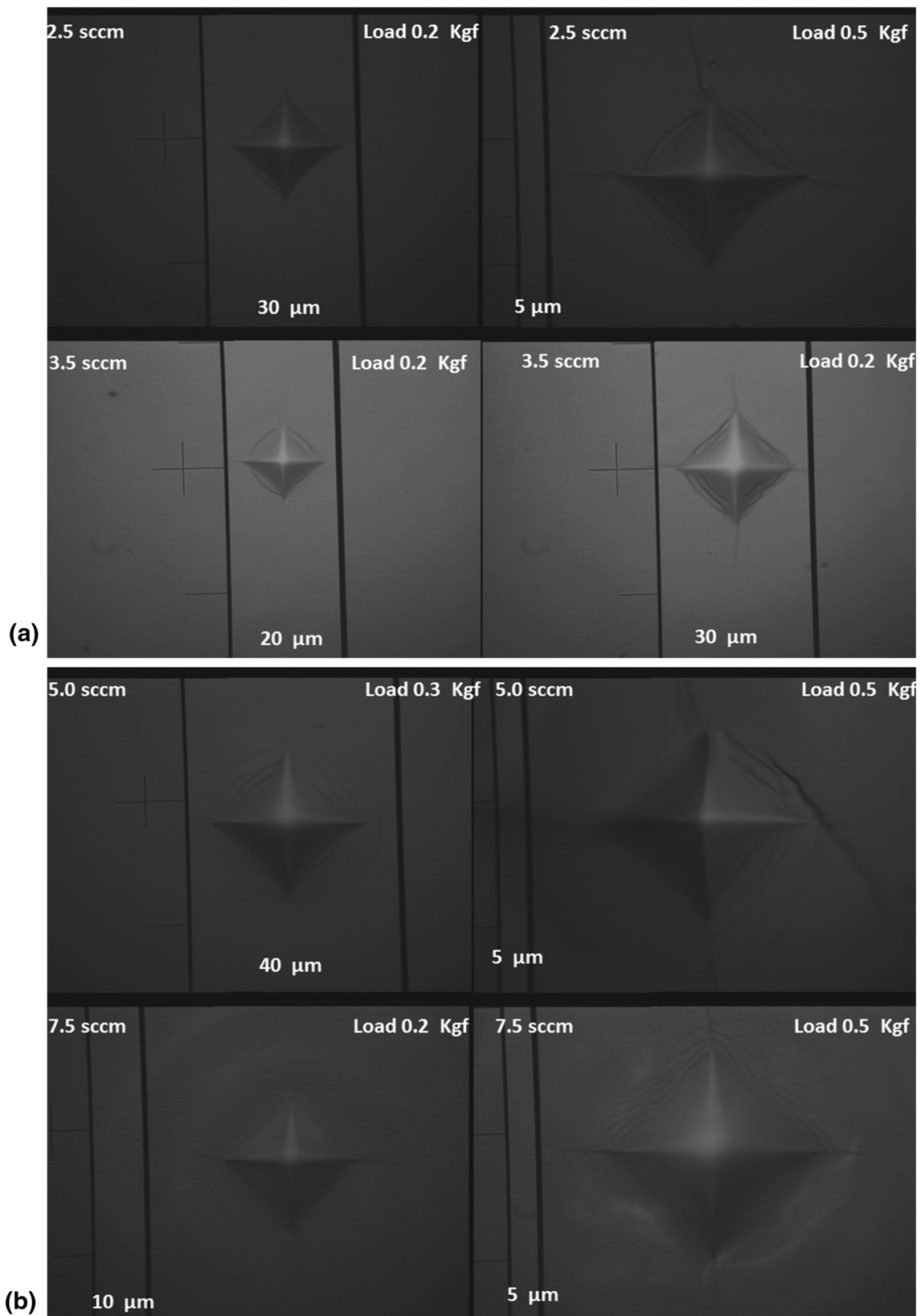
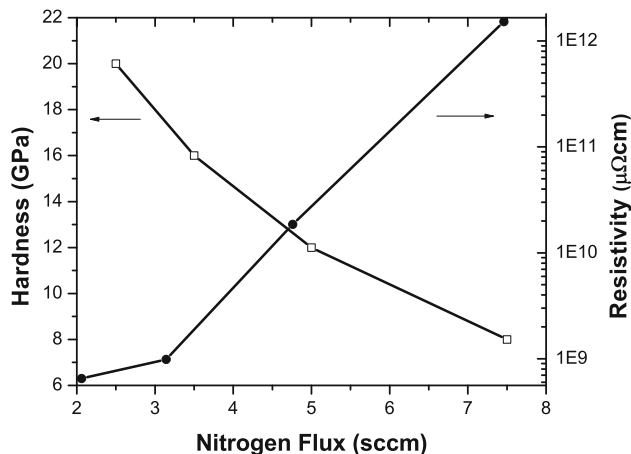
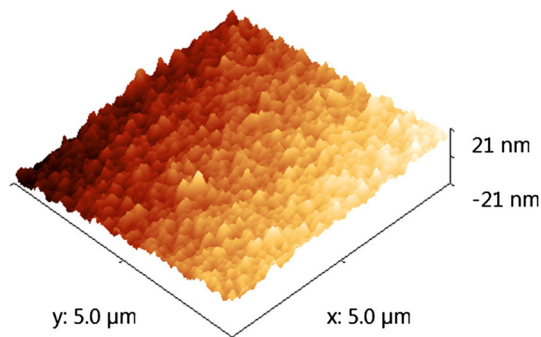


Fig. 5 Images of the indentations made to HfN coatings at two different loads: (a) HfN-2.5 and HfN-3.5 coatings and (b) HfN-5.0 and HfN-7.5 coatings

Table 1 Experimental data of the start and length of cracks, hardness, and fracture toughness of the coatings of HfN

Coatings	Critical loads of lateral crack formation, Kgf	Critical loads of radial crack formation, Kgf	Length of radial cracks, μm	Vickers hardness, GPa	Fracture toughness, $\text{MPa}\sqrt{\text{m}}$
HfN-2.5	0.2	0.5	29.3	20	0.22
HfN-3.5	0.2	0.2	16.8	16	0.23
HfN-5.0	0.3	0.5	29.1	12	0.29
HfN-7.5	0.5	0.2	17.9	8	0.30

**Fig. 6** Behavior of the hardness and electrical resistivity with the nitrogen flow rate variation**Fig. 7** Topography image of the HfN-2.5 coating, obtained by AFM

Acknowledgments

This work was supported by CONACYT under Projects 154516, as well as the Dirección General de Investigaciones of the Veracruzana University. The authors gratefully acknowledge the assistances received from Ing. Ayesha Margarita Courrech Arias of the Centro de Investigación en Micro y Nanotecnología de la Universidad Veracruzana by x-ray diffraction measurements performed, and from Dr. Angel Luis Rodríguez Morales of the Center of Applied Physics and Advanced Technology, Department of Molecular Engineering of Materials, Shock Waves Laboratory.

References

1. A.R. Shankar, U.K. Mudali, V. Chawla, and R. Chandra, Magnetron Sputter Deposition of Hafnium Nitride Coating On High Density

- Graphite and Niobium Substrates, *Ceram. Int.*, 2013, **39**(5), p 5175–5184
2. L.E. Koutsokeras, G.M. Matenoglou, and P. Patsalas, Structure, Electronic Properties and Electron Energy Loss Spectra of Transition Metal Nitride Films, *Thin Solid Films*, 2013, **528**, p 49–52
3. M. Yang, A.J. Allen, M.T. Nguyen, W.T. Ralston, M.J. MacLeod, and F.J. DiSalvo, Corrosion Behavior of Mesoporous Transition Metal Nitrides, *J. Solid State Chem.*, 2013, **205**, p 49–56
4. D. Kottfer, M. Ferdinandy, L. Kaczmarek, I. Maňková, and J. Beňo, Investigation of Ti and Cr Based PVD Coatings Deposited Onto HSS Co 5 Twist Drills, *Appl. Surf. Sci.*, 2013, **282**, p 770–776
5. A. Mkaddem, A.B. Soussia, and M.E. Mansori, Wear Resistance of CVD and PVD Multilayer Coatings When Dry Cutting Fiber Reinforced Polymers (FRP), *Wear*, 2013, **302**(1–2), p 946–954
6. A. Kafizas, C.J. Carmalt, and I.P. Parkin, CVD and Precursor Chemistry of Transition Metal Nitrides, *Coord. Chem. Rev.*, 2013, **257**(13–14), p 2073–2119
7. N. Jin, Y. Yang, X. Luo, and Z. Xia, Development of CVD Ti-Containing Films, *Prog. Mater. Sci.*, 2013, **58**, p 1490–1533
8. R. Hübner, Transition Metal Nitrides Thin Films Deposition Using a Dynamically Controlled Magnetron Sputtering Apparatus, *Surf. Coat. Technol.*, 2002, **158–159**, p 680–684
9. M.D. Jean, C.D. Liu, S.M. Chiu, and T.H. Chien, Modelling, Fabrication and Optimization for Hard Coatings of Deposited Ceramic Nitride Films Using a Magnetron Sputtering, *Phys. Proc.*, 2012, **32**, p 289–296
10. D. Martínez-Martínez, C. López-Cartes, A. Fernández, and J.C. Sánchez-López, Exploring the Benefits of Depositing Hard TiN Thin Films by Non-Reactive Magnetron Sputtering, *Appl. Surf. Sci.*, 2013, **275**, p 121–126
11. S.M. Borah, A.R. Pal, H. Bailung, and J. Chutia, Optimization of Plasma Parameters for High Rate Deposition of Titanium Nitride Films As Protective Coating On Bell-Metal By Reactive Sputtering in Cylindrical Magnetron Device, *Appl. Surf. Sci.*, 2008, **254**(18), p 5760–5765
12. Ph Roquiny, F. Bodart, and G. Terwagne, Colour Control of Titanium Nitride Coatings Produced by Reactive Magnetron Sputtering at Temperature Less Than 100 C, *Surf. Coat. Technol.*, 1999, **116–119**, p 278–283
13. E. Zalmezhad, A.D. Sarhan, and M. Hamdi, Investigating the Fretting Fatigue Life of Thin Film Titanium Nitride Coated Aerospace Al7075-T6 Alloy, *Mater. Sci. Eng. A*, 2013, **559**, p 436–446
14. J. Hernández-Torres, L. García-González, L. Zamora-Peredo, T. Hernández-Quiroz, A. Saucedo-Carvajal, P.J. García-Ramírez, and N. Flores-Ramírez, Analysis of Hardness of Nanocrystalline Coatings of Aluminum-Rich $\text{Ti}_{1-x}\text{Al}_x\text{N}$, *Bull. Mater. Sci.*, 2012, **35**(5), p 733–738
15. G. Berg, C. Friedrich, E. Broszeit, and K.H. Kloos, Comparison of Fundamental Properties of R.F.-Sputtered TiN_x and HfN_x Coatings on Steel Substrates, *Surf. Coat. Technol.*, 1995, **74–75**, p 135–142
16. T. Nozaki and Y. Hatano, Hydrogen Permeation Through a Pd/Ta Composite Membrane with a HfN Intermediate Layer, *Int. J. Hydrogen Energy*, 2013, **38**(27), p 11983–11987
17. L. Yuan, G. Fang, C. Li, C. Wang, N. Liu, L. Ai, Y. Cheng, H. Gao, and X. Zhao, Influence of N_2 Flow Ratio on the Properties of Hafnium Nitride Thin Films Prepared by DC Magnetron Sputtering, *Appl. Surf. Sci.*, 2007, **253**(20), p 8538–8542
18. W.D. Sproul, Hafnium Nitride Coatings Prepared by Very High Rate Reactive Sputtering, *Thin Solid Films*, 1984, **118**(3), p 279–284
19. J.S. Jeng, C.H. Liu, and J.S. Chen, Effects of Substrate Bias and Nitrogen Flow Ratio on the Resistivity, Composition, Crystal Structure, and Reflectance of Reactively Sputtered Hafnium-Nitride Film, *J. Alloys Compd.*, 2009, **486**(1–2), p 649–652

20. R. Nowak and S. Maruno, Surface Deformation and Electrical Properties of HfN Thin Films Deposited by Reactive Sputtering, *Mater. Sci. Eng. A*, 1995, **202**(1–2), p 226–237
21. M.H. Staia, D.G. Bhat, E.S. Puchi-Cabrera, and J. Bost, Characterization of Chemical Vapor Deposited HfN Multilayer Coatings on Cemented Carbide Cutting Tools, *Wear*, 2006, **261**(5–6), p 540–548
22. W. Wang, T. Nabatame, and Y. Shimogaki, Preparation of Conductive HfN by Post Rapid Thermal Annealing-Assisted MOCVD and Its Application to Metal Gate Electrode, *Microelectron. Eng.*, 2008, **85**(2), p 320–326
23. V. Kouznetsov, K. Macák, J.M. Schneider, U. Helmersson, and I. Petrov, A Novel Pulsed Magnetron Sputter Technique Utilizing Very High Target Power Densities, *Surf. Coat. Technol.*, 1999, **122**(2–3), p 290–293
24. B.E. Warren, X-Ray Studies of Deformed Metals, *Prog. Met. Phys.*, 1959, **9**, p 147–202
25. A. Morimoto, H. Shigeno, S. Morita, Y. Yonezawa, and T. Shimizu, Effect of Nitrogen Gas on Preparation of Ti-Al-N Thin Films by Pulsed Laser Ablation, *Appl. Surf. Sci.*, 1998, **127–129**, p 994–998
26. M. Stoehr, H.-S. Seo, I. Petrov, and J.E. Greene, Raman Scattering from Epitaxial HfN Layers Grown on MgO(001), *J. Appl. Phys.*, 2006, **99**, p 043507
27. A.M. Korsunsky, M.R. McGurk, S.J. Bull, and T.F. Page, On the Hardness of Coated Systems, *Surf. Coat. Technol.*, 1998, **99**(1–2), p 171–183
28. B.R. Lawn, A.G. Evans, and D.B. Marschall, Elastic/Plastic Indentation Damage in Ceramics: The Median/Radial Crack System, *J. Am. Ceram. Soc.*, 1980, **63**(9–10), p 574–581
29. E. Török, A.J. Perry, L. Chollet, and W.D. Sproul, Young's modulus of TiN, TiC, ZrN and HfN, *Thin Solid Films*, 1987, **153**(1–3), p 37–43
30. G.R. Anstis, P. Chantikul, B.R. Lawn, and D.B. Marshall, A Critical Evaluation of Indentation Techniques for Measuring Fracture Toughness: I, Direct Crack Measurements, *J. Am. Ceram. Soc.*, 1981, **64**(9), p 533–538
31. T. Kanzawa, N. Setojima, Y. Miyata, Y. Gotoh, H. Tsuji, and J. Ishikawa, Evaluation of Hafnium Nitride Thin Films Sputtered from a Hafnium Nitride Target, *Vacuum*, 2009, **83**(3), p 589–591
32. Ch-H Tsai, Y.-S. Lai, and J.S. Chen, Thermal Stability of Hafnium and Hafnium Nitride Gates on HfO₂ Gate Dielectrics, *J. Alloys Compd.*, 2009, **487**(1–2), p 687–692